Sensitivity of Pliocene climate simulations in MRI-CGCM2.3 to respective boundary conditions

Youichi Kamae[1,2], Kohei Yoshida[3], Hiroaki Ueda[1]

[1]Faculty of Life and Environmental Sciences, University of Tsukuba, Tsukuba, 305-8572, Japan
[2]Scripps Institution of Oceanography, University of California San Diego, La Jolla, 92093-0206, USA
[3]Meteorological Research Institute, Tsukuba, 305-0052, Japan

Correspondence to: Youichi Kamae (kamae.yoichi.fw@u.tsukuba.ac.jp)

Abstract. Accumulations of global proxy data are essential steps for improving reliability of climate model simulations for the Pliocene warming climate. In the Pliocene Model Intercomprison Project phase 2 (PlioMIP2), a part project of the Paleoclimate Modelling Intercomparison Project phase 4, boundary forcing data have been updated from the PlioMIP phase 1 due to recent advances in understanding of oceanic, terrestrial and cryospheric aspects of the Pliocene paleoenvironment. In this study, sensitivities of Pliocene climate simulations to the newly archived boundary conditions are evaluated by a set of simulations using an atmosphere-ocean coupled general circulation model, MRI-CGCM2.3. The simulated Pliocene climate is warmer than pre-industrial condition for 2.4 °C in global mean, corresponding to 0.6 °C warmer than the PlioMIP1 simulation by the identical climate model. Revised orography, lakes and shrunk ice sheets compared with the PlioMIP1 lead to local and remote influences including snow and sea ice albedo feedback, and poleward heat transport due to the atmosphere and ocean that result in additional warming over middle and high latitudes. The amplified higher-latitude warming is supported qualitatively by the proxy evidences, but is still underestimated quantitatively. Physical processes responsible for the global and regional climate changes should be further addressed in future studies under systematic intermodel and data–model comparison frameworks.

1 Introduction

Atmosphere-ocean coupled general circulation models (AOGCMs) have widely been used for climate projections on decadal to centennial timescales since the late 20th century. Recently, representations of large-scale climate state, its variability, and parameterized processes in the AOGCMs (e.g. cloud and convection) have been improved substantially (e.g. Reichler and Kim, 2008; Klein et al., 2013; Bellenger et al., 2014). A large ensemble of multiple climate models has contributed to addressing robust climate trends in the future projections (e.g. Xie et al., 2015). Model intercomparisons of the past climate changes and data–model comparisons are powerful frameworks for understanding physical processes responsible for climate change and variability and assessing reliability of the climate model projections (e.g. Braconnot et al., 2012; Masson-Delmotte et al., 2014).

Since the 1990s, globally warmed climate during the Pliocene (~5 to 3 Ma) has attracted much attention as a potential analogue for the ongoing global climate change (e.g. Masson-Delmotte et al., 2014). Previous modelling and proxy-based studies revealed that the Pliocene climate can be characterized by substantial global warming (2.7 to 4.0 °C) with anomalous zonal and meridional temperature gradients (Dowsett et al., 1992, 2010; Wara et al., 2005; Fedorov et al., 2013; Haywood et al., 2013, 2016a). Under the Pliocene Model Intercomprison Project phase 1 (PlioMIP1; Haywood et al., 2010, 2011), a part project of the Paleoclimate Modelling Intercomparison Project phase 3 (PMIP3), nine AOGCMs provided results of mid-Pliocene (3.264 to 3.025 Ma) climate simulations. A paleoenvironmental reconstruction project named the Pliocene Research Interpretation and Synoptic Mapping (PRISM) for PlioMIP1 (PRISM3D; Dowsett et al., 2010) provided global boundary condition dataset that is needed for performing the mid-Pliocene climate simulations. Through intercomparisons of multiple model results and data–model comparisons, large-scale climate pattern (Haywood et al., 2013), East Asian monsoon behaviour (R. Zhang et al., 2013), Atlantic Meridional Overturning Circulation (AMOC; Z.-S. Zhang et al., 2013), terrestrial climate (Salzmann et al., 2013) and oceanic conditions (Dowsett et al., 2012, 2013) were examined systematically. The PlioMIP1 was the first model intercomparison project comparing past modelled climate prescribed with proxy-based vegetation pattern that is distinct from the present-day condition. Numerous independent proxy data for the Pliocene (Haywood et al., 2016a) suggested predominant warming over the North Atlantic and the Arctic region and wetter climate over land (Salzmann et al., 2008). The climate simulations under the PlioMIP1 tended to underestimate the warming over the Northern Hemisphere middle and high latitudes (Salzmann et al., 2013; Dowsett et al., 2012, 2013) although the latitudinal warming gradient was reproduced qualitatively. Hill et al. (2014) pointed out a robust contribution of surface albedo due to changes in vegetation and ice sheets and ice-albedo feedbacks (sea ice and snow) to the warming amplifications over the polar regions.

Since the PRISM3D/PlioMIP1, newly archived proxy evidences have been integrated as PRISM4 dataset (Dowsett et al., 2016; hereafter D16) that is planned to be used for an ongoing modelling intercomparison project, PlioMIP phase 2 (PlioMIP2; Haywood et al., 2016b; hereafter H16b), a part project of PMIP4 (Kageyama et al., 2016). In the PRISM4/PlioMIP2, boundary conditions for the Pliocene climate simulations including orography and ice sheets have been updated. In addition, global lakes and soil data were newly included in the PRISM4 dataset. Numerous mega-lakes over land associated with the wetter terrestrial climate during the Pliocene were suggested to be important for simulating local and large-scale anomalous climate (Pound et al., 2014).

In the PlioMIP2, dynamical predictions of vegetation and lakes, changes in land and ocean topography, and change in the land–sea mask are recommended for the Pliocene climate simulations. However, the respective roles of the revised boundary conditions in the Pliocene climate simulations have not been addressed sufficiently. A set of sensitivity experiments with different combinations of modern and Pliocene boundary conditions is planned to be performed in the PlioMIP2. The respective roles of the boundary conditions can be evaluated by comparing results of the sensitivity runs. In this study, we conduct PlioMIP2 climate simulations by using an AOGCM, MRI-CGCM2.3, that was also used in the PlioMIP1 (Kamae

and Ueda, 2012; hereafter KU12). The results of the PlioMIP1 run, the PlioMIP2 run, and the PlioMIP2 sensitivity runs with swapped boundary conditions are used to examine respective roles of the updated boundary conditions. This study reports that the revised ice sheets in the high latitudes and global land properties including vegetation result in an amplified high latitude warming via direct influence, radiative feedback, and atmospheric and oceanic heat transports. The anomalous warming simulated in the PlioMIP2 protocol is more consistent with the proxy evidences than the PlioMIP1 run. Section 2 describes the data and methods including proxy-based boundary conditions and modelling strategy. Section 3 presents general characteristics of simulated Pliocene climate and compares it with the PlioMIP1 results. Section 4 examines the roles of atmospheric and oceanic meridional heat transports in the simulated middle and high latitude warming in the model. Section 5 compares modelled and reconstructed sea surface temperature (SST) and assess SST reproducibility of the model simulation. In Sect. 6, we present a summary and discussion of this study.

2 Data and Methods

2.1 Climate model

An AOGCM named MRI-CGCM2.3 (Yukimoto et al., 2006) was used for performing the PlioMIP2 experiments in this study. The model is identical to that used in the PlioMIP1 (KU12). Atmospheric model has a horizontally T42 resolution (~2.8°) and vertically 30 layers (model top is 0.4 hPa). Oceanic component is a Bryan-Cox-type ocean general circulation model with a horizontal resolution of 2.5° longitude and 2.0°–0.5° latitude and 23 layers (the deepest layer is 5000 m). Details of the atmosphere and ocean models can be found in Yukimoto et al. (2006) and KU12. Vegetation, lakes and atmospheric CO_2 concentration are prescribed in the model as boundary conditions (see Sect. 2.2) because the model does not predict vegetation, lakes, and carbon cycle (Table 1). Land scheme is simple biosphere model (SiB2; Sellers et al., 1986; Sato et al., 1989), which predicts soil water and surface heat budget. Parameters for the land scheme depend on 13 types of vegetation category (see Sect. 2.2). Lakes are treated in the land surface model as inland water in grid boxes with a drainage basin unconnected to oceans. The model predicts water budget for lakes, but the lake surface temperature is predicted by the heat budget at the water surface, assuming a slab with a thickness of 50 m (Yukimoto et al., 2006).

Although both the AOGCM and an atmosphere-only general circulation model were used in the PlioMIP1 (Kamae et al., 2011; KU12), we perform only the AOGCM simulations in this study according to the PlioMIP2 protocol (H16b). In KU12, a set of AOGCM simulations with and without flux adjustments (heat, fresh water flux and wind stress) were performed. In the present study, we only integrated the model without any flux adjustments (similar to AOGCM_NFA run in KU12).

2.2 Experimental designs for pre-industrial and Pliocene climate simulations

In addition to two core experiments (pre-industrial and Pliocene), a set of sensitivity experiments (Table 2) is also proposed in the PlioMIP2 (Table 3 in H16b). Alterations of soil and land–sea mask (e.g. the Bering Strait and the Canadian Arctic Archipelago) were recommended in the PlioMIP2. Due to technical difficulties, these alterations were not incorporated into

the current PlioMIP2 simulations. Due to the low resolution and the simple experimental setting (i.e. low computational cost), we can conduct all the set of simulations proposed in the PlioMIP2 (totally 12-type 500-yr long simulations; H16b). We also plan to conduct higher resolution and/or higher complexity PlioMIP2 simulations with a higher-resolution AOGCM and/or an Earth system model (see Sect. 6).

We can compare results of this study with the PlioMIP1 directly because the experimental setting for the PlioMIP2 pre-industrial run (Tables 1 and 2) is identical to the PlioMIP1 (KU12). In the pre-industrial run, CO_2, CH_4 and N_2O concentrations were set to be 280 ppmv, 760 ppbv and 270 ppbv, respectively. Ozone concentration in each month was derived from climatology in Wang et al. (1995). Orbital parameters were identical to the PlioMIP1 (Table 1). Modern land orography, lakes, and ice sheets of the MRI-CGCM2.3 (KU12; Figs. 1a, 2a) were used in the pre-industrial run. Vegetation pattern was derived from PRISM3D modern map converted into 13 types of SiB2 classification (Table 3 in KU12; Fig. 1a).

To simulate the Pliocene climate, the PRISM4 global paleoenvironmental dataset (D16) including atmospheric trace gases, orography, vegetation covers, ice sheets, and lakes are prescribed in the model. Pliocene orography was updated from the PRISM3D (Sohl et al., 2009) by considering mantle flow (Rowley et al., 2013) and glacial isostatic response of ice sheet loading (Raymo et al., 2011). We added anomalous orography (Pliocene minus modern) to the model's modern orography (Fig. 3) according to the "anomaly method" recommended in the PlioMIP2 (H16b). Direct proxy evidences for the Greenland and Antarctic ice sheets during the Pliocene were not available. The PRISM4 provided Greenland ice sheet data that is confined to high elevations in the East Greenland Mountains suggested by results of Pliocene Land Ice Sheet Model Intercomparison Project (Dolan et al., 2015; Koenig et al., 2015). According to proxy data for the Antarctic ice sheet (Naish et al., 2009; Pollard and DeConto, 2009), ice-free condition and the identical ice sheet estimate to the PRISM3D were assumed in the West and East Antarctica, respectively (D16; Figs. 1b, 3). The resultant prescribed ice sheets over the Greenland and Antarctica are smaller than that in KU12. We prescribed the Pliocene ice sheets by changing land orography (Fig. 1) and land cover (Fig. 3) over the ice sheets regions. Because the model does not predict dynamic vegetation, we prescribe vegetation pattern (Fig. 1b) that is identical to the PRISM3D/PlioMIP1 (Salzmann et al., 2008), according to the recommendation in H16b.

In addition to vegetation, global lake distribution during the Pliocene was also suggested to be distinct from the present day. Schuster et al. (2001, 2006) and Griffin (2006) suggested the existence of the African Megalakes existed during the Miocene and the Pliocene. Contoux et al. (2013) and Pound et al. (2014) pointed out an important role of the Pliocene lakes in the global climate through local atmosphere-land interaction and remote influences. The PRISM4 provides global lake area data (Pound et al., 2014) for the PlioMIP2 (Fig. 2). We prescribe the Pliocene lakes (Fig. 2b; Table 2) by adding anomalous areas of lakes (Fig. 2c) to model's modern lakes (the Caspian Sea, the Aral Sea, Lake Balkhash, Lake Chad and Lake Eyre; Fig. 2a).

In this paper, the results of six PlioMIP2 experiments (Table 2) are reported: pre-industrial run; Pliocene run; pre-industrial runs but with CO_2 concentration of 400 and 560 ppmv (hereafter E400 and E560 runs); pre-industrial run but with Pliocene ice sheets (Ei280 run); and pre-industrial run but with Pliocene orography, vegetation, and lakes (OVL) except over the ice sheets regions (hereafter Eo280 run). CH_4, N_2O, ozone, solar constant, orbital parameters are identical to the pre-industrial run (Table 1). Land orography, lake area, vegetation, land ice, atmospheric CO_2 concentration are altered in the Pliocene run from the pre-industrial run. Combinations of the boundary conditions are changed in the sensitivity runs so that the impacts of the individual components can be evaluated (Table 2; Sect. 2.3). A large spread remains in the assessment of the Pliocene CO_2 concentration (e.g. Raymo et al., 1996; Seki et al., 2010; D16). Although 400 ppmv of CO_2 concentration is prescribed in the Pliocene run, other concentrations are also used in the other sensitivity runs (H16b). In this paper, we examine the results of simulations with CO_2 concentration of 280, 400 and 560 ppmv (Table 2).

The results are also compared with PlioMIP1 run conducted in KU12 (Table 2). Pliocene lakes were set to be identical to the modern. The PRISM3D-based vegetation (Salzmann et al., 2008) was also prescribed in the PlioMIP1 Pliocene run (Fig. 1b). A prescribed CO_2 concentration of 405 ppmv was slightly higher than the PlioMIP2.

The initial condition for the PlioMIP2 runs is identical to the pre-industrial run: 31 December of the PlioMIP1 control run (in NFA_AOGCM) after 500-yr spin up (Fig. 3b in KU12). The model is integrated for another 500 years with swapped boundary conditions and the last 50 years are used for analyses. Note that reconstructed deep ocean temperature was added to the initial condition of the PlioMIP1 Pliocene run (KU12), distinct to the PlioMIP2. Despite the difference in the initial deep ocean temperature, ocean circulation and SST after the 500-yr integrations are generally similar between the two (see Sects. 3.3, 4, 5).

2.3 Respective roles of boundary conditions

In the PlioMIP2, relative contributions of the boundary conditions to climate anomalies (e.g. global mean warming) can be evaluated by comparing the set of sensitivity experiments (H16b). In this study, we use the six PlioMIP2 simulations (Table 2) and evaluate the respective contributions by following Eqs. (1–6):

$$All = [\mathrm{Eoi400}] - [\mathrm{E280}] , \quad (1)$$

$$CO2 = [\mathrm{E400}] - [\mathrm{E280}] , \quad (2)$$

$$OVL = [\mathrm{Eo280}] - [\mathrm{E280}] , \quad (3)$$

$$Ice\ Sheet = [\mathrm{Ei280}] - [\mathrm{E280}] , \quad (4)$$

$$Sum = CO2 + OVL + Ice\ Sheet , \quad (5)$$

$$Residual = All - Sum , \quad (6)$$

where [] represents the experiment name (Table 2). E280 and Eoi400 indicate the pre-industrial and Pliocene runs, respectively. Difference of results between Eo280 and E280 run corresponds to effect of differences in OVL. Sum of Eqs. (2–4) is used as a reconstruction of Eq. (1). By Eqs. (5, 6), we can compare the simulated climate anomaly between the Pliocene run and the pre-industrial and its reconstruction. *Residual* (Eq. 6) indicates a nonlinear effect of combination of the boundary conditions associated with nonlinearity in forcing-response relationship (e.g. Shiogama et al., 2013). This decomposition method is not identical to that recommended in H16b. While decomposed relative contributions could be dependent on the choice of quantifying methods, *Residual* term shown in this study is generally minor to *All* (see Sect. 3), suggesting an effectiveness of the decomposing method used in this study.

3 Results

3.1 Global mean warming in Pliocene run

First, we compare global mean surface air temperature (SAT) change between the simulations. Figure 4 shows the time evolution of the global mean SAT during the 500-yr model integrations. Compared with the pre-industrial run, identical to the PlioMIP1 control simulation (KU12), all the experiments show higher global mean SAT. The Pliocene run shows a more stable long-term trend (year 70–500) than other sensitivity runs prescribed with the OVL (Eo280) or CO_2 (E400). The doubling CO_2 experiment (E560) shows a long-term warming trend and the resultant warming for the last 50 years accounts for 2.8 °C (Table 3). In the E400 run prescribed with CO_2 concentration of 400 ppmv, global mean warming accounts for 1.7 °C that is the largest contributor to the Pliocene warmth among the boundary conditions (68 %; Table 3), consistent with Willeit et al. (2013). Here *Sum* (2.5 °C) can reconstruct *All* (2.4 °C) quantitatively. Contributions of *Ice Sheet* and *OVL* are 12 and 20 %, respectively. Compared with the PlioMIP1 run (1.8 °C), the PlioMIP2 Pliocene run shows a larger warming (+39 %, 0.7 °C) although the prescribed CO_2 concentration (400 ppmv) is slightly lower (405 ppmv in PlioMIP1). In the next section, we compare spatial patterns of the results and decompose respective contributions of the individual boundary conditions.

3.2 Regional changes in temperature and precipitation

Figure 5 shows spatial distributions of annual mean SAT anomalies averaged over the last 50 years. Similar to the PlioMIP1 run (KU12; Haywood et al., 2013), the Pliocene anomaly exhibits a polar amplification of surface warming (i.e. warming peaks over the high latitudes including Greenland and the Antarctica). While land surface warming is generally larger than the ocean surface warming (in response to CO_2 forcing; Fig. 5b; Manabe et al., 1991; Kamae et al., 2014), regional differences in SAT change (weak warming compared with surrounding areas) are found over southern North America, tropical Africa, Indian subcontinent, and eastern Siberia, similar to the PlioMIP1 (KU12). Zonally averaged SAT change exhibits (1) minimum warming over the Southern Hemisphere middle latitude; (2) moderate warming over the tropics; and (3) warming peaks over the Southern and Northern Hemisphere high latitudes (Fig. 6a). SST also exhibits the inter-

hemispheric warming asymmetry (Figs. 5e, 6b; see Sect. 3.3) and warming peak in the Northern Hemisphere mid-to-high-latitude (particularly in the eastern North Pacific and North Atlantic; Figs. 5e, 6b). Here *Sum* of zonal mean SAT, SST and other variables (e.g. precipitation) are similar to *All* (Fig. 6), indicating a limited *Residual* term in the zonal mean (Eq. 6). The effectiveness of reconstruction of *All* by *Sum* suggests that characteristics of the Pliocene climate anomaly can be decomposed into the individual contributions by Eq. (5). Note that *Sum* tends to underestimate (overestimate) the Southern (Northern) Hemisphere middle and high latitude warming, suggesting an importance of nonlinear effects (see Sect. 4).

Compared to the PlioMIP1, the Pliocene run exhibits a larger warming over Antarctica and the Northern Hemisphere middle and high latitudes (Fig. 6a), resulting in the larger increase in global mean SAT (Sect. 3.1). In addition to the less ice sheets over Greenland and West Antarctica, other factors also contribute to the polar amplification of surface warming (Figs. 5, 6a). The decomposition based on the sensitivity runs (Sect. 2.3) indicates that all the boundary conditions contribute to the polar warming (Figs. 5, 6a). Contributions of *OVL* and *CO2* to the zonal mean polar warming are dominant (Figs. 5b, c, 6a). Here *OVL* is the largest contributor to the latitudinal difference in the Northern Hemisphere warming and the inter-hemispheric warming contrast (Fig. 6a). Although spatially smooth CO_2 radiative forcing also leads to the polar amplification (Fig. 6a; e.g. Serreze and Barry, 2011; Hill et al., 2014), *OVL* effect dominates the meridional warming contrast. Note that *CO2* is the largest contributor to the global mean Pliocene warming (Sect. 3.1). In Sect. 5, we assess reproducibility of the SST in the PlioMIP2 and 1 runs by comparing with proxy-based estimate.

Figures 7 and 6e show change in surface albedo and its zonal mean. Increasing albedo over North America middle latitude and eastern Siberia due to change in vegetation (boreal forest in modern but grassland in the Pliocene; Fig. 1; Haywood et al., 2013; Hill et al., 2014), a part of *OVL* effect, contributes to the regional difference in the SAT change (Figs. 5c, 7c). Over the Northern Hemisphere high latitude, the reduced ice sheets (Figs. 1, 3) and a reduction of surface albedo (Figs. 6e, 7c) due to northward shift of boreal forest (deciduous conifer, tundra and bare soil regions over northern Canada and northeastern Eurasia; Fig. 1) result in regional warming (Fig. 5c, d). Surface snow cover (not shown) also affects partly the land surface albedo. The high latitude SAT is more sensitive to imposed albedo change due to the altered vegetation cover (Fig. 1) than low latitude (Davin and de Noblet-Ducoudré, 2010), consistent with the substantial Arctic warming found in current study (Fig. 5) and previous studies (Willeit et al., 2013; Zhang and Jiang, 2014). Decreasing albedo over the high latitude ocean (the Arctic and Antarctic Ocean) corresponds to sea ice reductions (Fig. 6e, f) that are larger than the PlioMIP1 (Fig. 6f; Howell et al., 2016). Sea ice and snow albedo feedback contributes to the differential polar and global-mean warming between the two runs. Over semi-arid and arid land regions, local SAT change corresponds well with precipitation change (Fig. 8; e.g. Kamae et al., 2011). *OVL* leads to increased precipitation over western North America, tropical Africa, and Indian subcontinent (Fig. 8c), resulting in surface cooling (Fig. 5c) via changing surface heat fluxes (not shown).

The precipitation response in the PlioMIP2 run, dominated by *OVL* effect, is generally larger than the PlioMIP1 run (Figs. 6c, 8; Fig. 7g in KU12). The anomalous middle and high latitude warming associated with the altered boundary conditions (e.g. darker land surface due to northward shift of boreal forest; Fig. 1) could affect the large-scale precipitation pattern via

changing atmospheric circulations (Sect. 3.3). For example, tropical precipitation associated with Intertropical Convergence Zones (ITCZs) is sensitive to inter-hemispheric warming asymmetry (e.g. Braconnot et al., 2007). In the tropical Atlantic, inter-hemispheric warming gradient (warmer in the North Atlantic than the South Atlantic; Fig. 5g) affects the Atlantic and African ITCZ precipitation (Fig. 8c; e.g. Zhang and Delworth, 2006). In addition, regional alterations of land surface condition can also affect local precipitation. The expansions of the lakes over tropical Africa and mid-latitude western North America (Fig. 2c) reduce surface sensible heat flux and enhance local hydrological cycle (e.g. surface evaporation and precipitation; Pound et al., 2014). The enhanced precipitation over the semi-arid regions is an important factor for simulating the Pliocene vegetation pattern (Kamae and Ueda, 2011; Contoux et al., 2013; Pound et al., 2014). The tropical precipitation changes may also be associated with changes in regional land–sea temperature contrast and seasonal monsoon circulations (e.g. R. Zhang et al., 2013).

3.3 Meridional overturning circulation

The surface temperature (SAT and SST) shows warming peaks over the middle and high latitudes and the inter-hemispheric warming asymmetry (Figs. 5, 6a, b). The warming peaks in the PlioMIP2 are larger than that the PlioMIP1 (Fig. 6a). Both changes in precipitation (Figs. 6c, 8) and cloud amount (not shown) show inter-hemispheric asymmetries (larger increase in the Northern Hemisphere than the Southern Hemisphere), suggesting a change in large-scale atmospheric circulation (e.g. Kang et al., 2009). Figure 9 shows changes in atmospheric mean meridional circulation (MMC) determined by mass stream function (MSF). The MMC, one of the important factors for the Pliocene climate anomaly (Chandler et al., 1994; Brierley et al., 2009; Brierley and Fedorov, 2010; Kamae et al., 2011; Sun et al., 2013; Li et al., 2015), shows a larger change compared with the PlioMIP1 (Fig. 6d). The MMC change is largely characterized as enhanced (weakened) Southern (Northern) Hemisphere Hadley cell, northward shift of the tropical Hadley cells, and enhanced mid-latitude cell over the Northern Hemisphere (Figs. 6d, 9a). The boundary of the two Hadley cells and northern edge of the northern cell (determined by signs of MSF at 500 hPa level; Fig. 6d) shift northward for 7.2° and 2.0°, respectively, and the mid-latitude cell is enhanced for 41 %, largely according to the *OVL* effect (Figs. 6d, 9c). The change in the Hadley circulation is consistent with the PlioMIP1 qualitatively but larger quantitatively, suggesting an anomalous meridional heat transport due to the MMC (see Sect. 4).

The simulated SST anomaly shows the remarkable meridional warming gradient, particularly over the Atlantic (Fig. 5), resulting from a substantial anomaly in the AMOC. Climatological AMOC in the pre-industrial run shown in Fig. 10 (4.2 Sv) is weaker than observations (e.g. Buckley and Marchall, 2016) and other PlioMIP1 models (Z.-S. Zhang et al., 2013). Note that AMOC simulated in MRI-CGCM2.3 shown in Z.-S. Zhang et al. (2013) is a result of simulation with the flux adjustments (KU12). The Pliocene AMOC simulated in the PlioMIP2 (without any flux adjustments) is quite stronger (+15 Sv) than the pre-industrial run, suggesting an intensified northward heat transport due to the Atlantic. The AMOC change dominates in *OVL* (+14.5 Sv; Fig. 10c) and enhancement due to *CO2* is moderate. Here change in sea surface density flux

over the North Atlantic (Speer and Tziperman, 1992) is one of possible controlling factors for the *OVL*-induced AMOC change. In response to the prescribed boundary conditions, changes in air and surface water temperature, atmospheric humidity, cloud cover, and surface wind speed can influence on sea surface heat fluxes (sensible heat flux, latent heat flux, and longwave and shortwave radiative flux). In addition, changes in river runoff, sea ice melt, and precipitation minus evaporation can affect sea surface salinity. These heat and salinity fluxes possibly modulate AMOC strength in the Pliocene climate. We plan to address physical processes contributing to the *OVL*-induced stronger AMOC in a separated paper. In the next section, we discuss possible factors contributing to the substantial higher latitude warming found in the Pliocene run.

4 Mid- and high-latitude warming and meridional heat transport

The PlioMIP2 run shows the larger middle and high latitude warming over the Northern Hemisphere (9 °C at 75° N; Fig. 6a) compared with the PlioMIP1 run. Hill et al. (2014) evaluated the contributions of factors for the polar amplification by using eight PlioMIP1 models. Despite substantial inter-model spreads, strong warming due to reduced surface albedo was robustly found in all the models and relative contribution of meridional heat transport (due to the atmosphere and ocean) was minor. Figure 6g shows anomalous northward heat transport due to the atmosphere. Over the Southern Hemisphere high latitude and tropics to Northern Hemisphere middle latitude, anomalous southward heat transport can be found while the atmospheric heat transport is positive (northward) over the Southern Hemisphere middle latitude (30° S–55° S). The tropical southward heat transport is largely consistent with the MMC change (i.e. the intensified and weakened Southern and Northern Hemisphere Hadley cells; Figs. 6d, 9). The southward heat transport over the Southern Hemisphere high latitude contributes to the Antarctic amplification in the Pliocene run (6–7 °C over 70° S–90° S).

Generally, *OVL* effect dominates and *CO2* and *Ice Sheet* effects are minor to the total change in the atmospheric heat transport. Over 50° N–70° N, *OVL* and *Ice Sheet* enhance northward heat transport, contributing to the Arctic warming (70° N–80° N). Here changes in MMC over 50° N–70° N are limited in these experiments (Fig. 6d), implying an important role of mid-latitude eddies. Changes in meridional temperature gradient in the upper troposphere and near the surface (e.g. Li et al., 2015) are possible factors for the anomalous mid-latitude eddy activity (e.g. Ulbrich et al., 2009). *OVL* effect contributes to an enhanced (a reduced) meridional temperature gradient in the upper troposphere (near the surface; Fig. 6a), similar to results of PlioMIP1 AOGCMs (Figs. 6 and 7 in Li et al., 2015). Such temperature changes imply a possible intensification of mid-latitude eddy activity (e.g. Mizuta, 2012). In addition, orography changes as parts of *OVL* and *Ice Sheet* effects (Fig. 3) can also affect mid-latitude atmospheric circulation and associated meridional heat transport. Note that nonlinear *Residual* term is remarkable in the northward heat transport. The northward heat transport is quite limited in the PlioMIP1 run (Fig. 6g), consistent with the difference in the high latitude warming between the PlioMIP2 and 1 (PlioMIP2 run shows stronger warming than PlioMIP1; Fig. 6a).

The simulated AMOC is much stronger than the pre-industrial run (Sect. 3.3), suggesting a substantial role in the North Atlantic warming during the Pliocene. Figure 6h shows northward heat transport due to the Atlantic Ocean. In contrast to

divergent responses among the PlioMIP1 models (Z.-S. Zhang et al., 2013), northward heat transport is enhanced substantially over the Northern Hemisphere (EQ–60° N). The enhanced heat transport is dominated by the *OVL* effect, consistent with the stronger AMOC found in the *OVL* (Fig. 10c). The stronger AMOC is also consistent with the substantial meridional SST gradient over the Atlantic (Fig. 5e), contributed by *OVL* and *CO2* (Fig. 5g, f). The enhanced mid-to-high-latitude warming is supported qualitatively by proxy-based SST reconstruction (Sect. 5).

The anomalous mid-to-high-latitude warming in the PlioMIP2 run is forced by the altered boundary conditions (Sect. 2.2) and is amplified/dampened by climate feedbacks and anomalous heat transports. As shown above, the impacts of CO_2 forcing and the Greenland ice sheet are relatively limited (Figs. 5d, 6a, b), suggesting the importance of *OVL* in the mid-to-high-latitude warming including the North Atlantic and the eastern North Pacific (Fig. 5g). Note that *Sum* overestimates the sea ice reduction and surface warming over the Northern Hemisphere high latitude simulated in *All* (Fig. 6a, b, f). In response to the strong external forcing including *CO2* and *OVL*, sea ice concentration can be 0 % at the edge of sea ice cover in the control climate (Howell et al., 2015). The limited sea ice concentration in the pre-industrial run is one of the possible reasons for the nonlinear relationship between forcing and sea ice reduction. Further analyses of relative contributions and inter-model consistency of cloud and surface albedo, longwave radiation, meridional heat transport due to atmosphere and individual ocean basins by using PlioMIP2 multi models may contribute to improve understanding of the physical mechanisms responsible for the Pliocene polar amplification.

5 Data–model comparison of SST

The Pliocene AMOC is apparently distinct from the pre-industrial run (Fig. 10), resulting in the anomalous northward heat transport due to the Atlantic Ocean (Fig. 6h). Here the larger North Atlantic warming (3–7 °C in 30° N–70° N; Fig. 5e) in the PlioMIP2 Pliocene run than the PlioMIP1 implies a better reproducibility of the mid-to-high-latitude SST warming that was robustly underestimated among the PlioMIP1 multi models (Dowsett et al., 2013). Figure 11 shows comparison of simulated SST and PRISM3D proxy-based SST reconstruction during the Pliocene (Dowsett et al., 2009). Note that the PRISM4 SST reconstruction is not updated (Dowsett et al., 2016) since PRISM3D. The SST reconstruction is characterized as extremely high SST in the North Atlantic high latitude, low-to-mid-latitude warming gradient (limited change in the tropics and warming in the middle latitude, respectively), and remarkable warming in mid-latitude coastal areas (off the west coast of North America and South America, and off the east coast of the Eurasian Continent; Dowsett et al., 2009, 2013).

Figures 11 and 12 compare SST biases found in the PlioMIP2 and 1. Generally, both the PlioMIP2 and 1 tend to underestimate the mid-to-high-latitude warming suggested by proxy records (blue circles in Fig. 11a; Haywood et al., 2013). However, the large part of underestimation of the mid-to-high-latitude warming is reduced substantially in the PlioMIP2 run (green circles in Fig. 11b). In contrast to the remarkable underestimation (SST bias is larger than 4 °C; Fig. 12) of the mid-latitude warming (the North Atlantic, off the west coast of North America and South America, and off the east coast of the Eurasian Continent) in the PlioMIP1 (black circles in Figs. 11 and 12), the SST biases are much reduced in the PlioMIP2 run

(Figs. 11b and 12). From a zonal-mean perspective, the larger mid-to-high-latitude warming (Fig. 6a, b) in the PlioMIP2 run is more consistent with the proxy evidences than the PlioMIP1 (Figs. 11b, 12). Note that SST bias (8.9–12 °C in 69° N–81° N) over the North Atlantic high latitude (open blue circles in Figs. 11 and 12) is still not reduced in this simulation. This data–model discord was also consistently found in PlioMIP1 multiple climate models (Dowsett et al., 2013). Haywood et al. (2013) noted that this substantial data–model discord is highly dependent on mean annual temperature estimate based on geochemically-based proxy data and is not derived from faunal based estimates of cold/warm month means. They suggested that we should not rely on this data–model discord too much until more variety of proxy records is available from more locations in the high latitude North Atlantic. In addition to the possible issue on the proxy-based estimate, modelled biases in AMOC and/or sea ice can also contribute to the North Atlantic data–model discord.

6 Summary and discussion

The PlioMIP2 simulations are conducted by using MRI-CGCM2.3 and prescribing the updated Pliocene paleoenvironmental dataset, called PRISM4. The Pliocene climate simulation with the identical model but with slightly revised boundary conditions from the PlioMIP1 results in the remarkable global-mean warming with the anomalous mid-to-high-latitude warming. The sensitivity experiments with swapped boundary conditions can largely reconstruct the modelled Pliocene climate anomalies, suggesting the linear additivity of the Pliocene climate simulation. However, linear additivity does not hold so well for regional climate responses including sea ice reduction over the high latitude oceans. The anomalous Northern Hemisphere higher-latitude warming can be understood as sum of direct response to the external forcing and associated climate feedbacks. The prescribed external forcing including CO_2, reduced ice sheets, and shortwave absorption due to the Arctic boreal forest contribute substantially to the higher-latitude warming. In addition, the anomalous northward heat transport associated with the large-scale atmospheric circulations and intensified AMOC, and snow and sea ice albedo feedback are also essential factors. The resultant anomalous warming over the mid-latitude ocean is more consistent with the proxy data than the PlioMIP1 simulation. However, the extremely warm condition over the Arctic to high-latitude North Atlantic region is not reproduced in this model.

The relative contributions to the polar amplification diverged substantially among multi models except those of surface albedo and CO_2 (Hill et al., 2014). In the PlioMIP1, the respective roles of the atmospheric and oceanic heat transports in the latitudinal warming gradient were not evaluated sufficiently. The intensified southern Hadley cell and a northward shift of the tropical cells can be confirmed in most of the PlioMIP1 models (Sun et al., 2013; Li et al., 2015). Both the PlioMIP1 multi models and the MRI-CGCM2.3 PlioMIP2 run show the predominant latitudinal contrast of surface warming over the Northern Hemisphere and the meridionally asymmetric change in the Hadley cells. However, the anomalous Hadley circulation transports heat southward, indicating that the change in the Hadley circulation is not a factor but can be understood as a result of the change in atmospheric meridional warming gradient (Li et al., 2015). Further analyses of the surface processes over land and ocean and three-dimensional atmospheric and oceanic processes (e.g. oceanic heat transport,

atmospheric heat transport due to mean circulations, stationary eddies, transient eddies, feedback associated with ice albedo, water vapour, cloud, and lapse rate; e.g. Serreze and Barry, 2011; Pithan and Mauritsen, 2014; Yoshimori et al., 2014) are needed to evaluate the respective contributions to the polar amplified climate in the Pliocene.

The simulated enhancement of the AMOC contributes to the North Atlantic warming in the Pliocene run. Z.-S. Zhang et al. (2013) revealed that none of the PlioMIP1 models simulated the substantial enhancement of the AMOC implied by the proxy records (e.g. Raymo et al., 1996; Robinson, 2009). This is inconsistent with the current study because Z.-S. Zhang et al. (2013) introduced the results of flux-adjusted version of the MRI-CGCM2.3 model run (KU12). The MRI-CGCM2.3 without any flux adjustments simulates the much enhanced AMOC both in the PlioMIP1 and 2 settings (Fig. 6h). The current study points out the importance of *OVL* effect to the enhanced AMOC, but does not identify physical processes contributing to the drastic change. We plan to clarify the physical mechanisms by comparing spatial and vertical distribution of salinity, heat and fresh water budget at sea surface, and its role in the AMOC strengths in the Pliocene run. Results of such analyses will be presented in a separated paper. Recent studies suggested that oceanic gateways (e.g. the Bering Strait; Hu et al., 2015) and bathymetry potentially contribute to past warming/cooling climate anomalies (e.g. Motoi et al., 2005; Robinson et al., 2011; Brierley and Fedorov, 2016). Sensitivity of simulated Pliocene climate to the PRISM4-based reconstructions of land–sea mask and bathymetry (D16) should be further evaluated in multi-model frameworks.

Assessment of regional climate properties (e.g. the Asian monsoon; R. Zhang et al., 2013) in the PlioMIP2 results is one of the remaining issues. Detailed data–model comparison of the oceanic and terrestrial climate should also be conducted to evaluate systematic biases in the PlioMIP2 model ensemble. The model experiment presented in the current study did not implement changes in the land–sea mask, soil, dynamic vegetation, and dynamic lakes. Implementation of the proxy-based soil properties as a boundary condition potentially affects the simulated Pliocene climate via changing surface and atmospheric energy and water budget (Pound et al., 2014). Low resolution models are not suitable for simulating the regional atmospheric circulation and hydrological cycle associated with land orography (e.g. Xie et al., 2006). We plan to conduct more complex PlioMIP2 simulations that are more consistent with the proxy-based reconstructions by incorporating all the requested boundary conditions to an Earth system model or a high resolution AOGCM. Further complex and fine resolution modelling, multiple model intercomparison, and data–model comparisons could advance understanding of the factors for the Pliocene warming climate.

Acknowledgements

We thank anonymous reviewers for giving constructive comments. The authors acknowledge PRISM4 and PRISM3D project members for archiving and providing global paleoenvironmental datasets for the Pliocene climate model simulations. We also thank A. M. Haywood and A. M. Dolan for coordinating the model intercomparison project, PlioMIP2.

References

Bellenger, H., Guilyardi, E., Leloup, J., Lengaigne, M., and Vialard, J.: ENSO representation in climate models: from CMIP3 to CMIP5, Clim. Dyn., 42, 1999–2018, 2014.

Braconnot, P., Otto-Bliesner, B., Harrison, S., Joussaume, S., Peterchmitt, J.-Y., Abe-Ouchi, A., Crucifix, M., Driesschaert, E., Fichefet, Th., Hewitt, C. D., Kageyama, M., Kitoh, A., Loutre, M.-F., Marti, O., Merkel, U., Ramstein, G., Valdes, P., Weber, L., Yu, Y., and Zhao, Y.: Results of PMIP2 coupled simulations of the Mid-Holocene and Last Glacial Maximum – Part 2: feedbacks with emphasis on the location of the ITCZ and mid- and high latitudes heat budget, Clim. Past, 3, 279-296, doi:10.5194/cp-3-279-2007, 2007.

Braconnot, P., Harrison, S. P., Kageyama, M., Bartlein, P. J., Masson-Delmotte, V., Abe-Ouchi, A., Otto-Bliesner, B., and Zhao, Y.: Evaluation of climate models using palaeoclimatic data, Nature Clim. Change, 2, 417–424, 2012.

Brierley, C. M. and Fedorov, A. V.: Relative importance of meridional and zonal sea surface temperature gradients for the onset of the ice ages and Pliocene-Pleistocene climate evolution, Paleoceanography, 25, PA2214, 2010.

Brierley, C. M. and Fedorov, A. V.: Comparing the impacts of Miocene–Pliocene changes in inter-ocean gateways on climate: Central American Seaway, Bering Strait, and Indonesia, Earth Planet. Sci. Lett., 444, 116–130, 2016.

Brierley, C. M., Fedorov, A. V., Lui, Z., Herbert, T., Lawrence, K., and LaRiviere, J. P.: Greatly expanded tropical warm pool and weakened Hadley circulation in the early Pliocene, Science, 323, 1714–1718, 2009.

Buckley, M. W. and Marshall, J.: Observations, inferences, and mechanisms of the Atlantic Meridional Overturning Circulation: A review, Rev. Geophys., 54, 5–63, 2016.

Chandler, M. A., Rind, D., and Thompson, R. S.: Joint investigations of the middle Pliocene climate II: GISS GCM Northern Hemisphere results, Global Planet. Change, 9, 197–219, 1994.

Contoux, C., Jost, A., Ramstein, G., Sepulchre, P., Krinner, G., and Schuster, M.: Megalake Chad impact on climate and vegetation during the late Pliocene and the mid-Holocene, Clim. Past, 9, 1417–1430, 2013.

Davin, E. L. and de Noblet-Ducoudré, N.: Climatic impact of global-scale deforestation: Radiative versus nonradiative processes, J. Clim., 23, 97–112, 2010.

Dolan, A. M., Hunter, S. J., Hill, D. J., Haywood, A. M., Koenig, S. J., Otto-Bliesner, B. L., Abe-Ouchi, A., Bragg, F., Chan, W.-L., Chandler, M. A., Contoux, C., Jost, A., Kamae, Y., Lohmann, G., Lunt, D. J., Ramstein, G., Rosenbloom, N. A., Sohl, L., Stepanek, C., Ueda, H., Yan, Q., and Zhang, Z.: Using results from the PlioMIP ensemble to investigate the Greenland Ice Sheet during the mid-Pliocene warm period, Clim. Past, 11, 403–424, 2015.

Dowsett, H. J., Cronin, T. M., Poore, R. Z., Thompson, R. S., Whatley, R. C. and Wood, A. M.: Micropaleontological evidence for increased meridional heat transport in the North Atlantic Ocean during the Pliocene, Science, 258, 1133–1135, 1992.

Dowsett, H., Robinson, M., and Foley, K.: Pliocene three-dimensional global ocean temperature reconstruction, Clim. Past, 5, 769-783, 2009.

Dowsett, H. J., Robinson, M. M., Haywood, A. M., Salzmann, U., Hill, D., Sohl, L., Chandler, M., Williams, M., Foley, K. and Stoll, D. K.: The PRISM3D paleoenvironmental reconstruction, Stratigraphy, 7, 123–139, 2010.

Dowsett, H. J., Robinson, M. M., Haywood, A. M., Hill, D. J., Dolan, A. M., Stoll, D. K., Chan, W.-L., Abe-Ouchi, A., Chandler, M. A., and Rosenbloom, N. A.: Assessing confidence in Pliocene sea surface temperatures to evaluate predictive models, Nature Clim. Change, 2, 365–371, 2012.

Dowsett, H. J., Foley, K. M., Stoll, D. K., Chandler, M. A., Sohl, L. E., Bentsen, M., Otto-Bliesner, B. L., Bragg, F. J., Chan, W.-L., Contoux, C., Dolan, A. M., Haywood, A. M., Jonas, J. A., Jost, A., Kamae, Y., Lohmann, G., Lunt, D. J., Nisancioglu, K. H., Abe-Ouchi, A., Ramstein, G., Riesselman, C. R., Robinson, M. M., Rosenbloom, N. A., Salzmann, U., Stepanek, C., Strother, S. L., Ueda, H., Yan, Q., and Zhang, Z.: Sea surface temperature of the mid-Piacenzian Ocean: A data-model comparison, Sci. Rep., 3, 2013, 2013.

Dowsett, H. J., Dolan, A., Rowley, D., Pound, M., Salzmann, U., Robinson, M., Chandler, M., Foley, K., and Haywood, A.: The PRISM4 (mid-Piacenzian) palaeoenvironmental reconstruction, Clim. Past Discuss., doi:10.5194/cp-2016-33, 2016.

Fedorov, A. V., Brierley, C. M., Lawrence, K. T., Liu, Z., Dekens, P. S., and Ravelo, A. C.: Patterns and mechanisms of early Pliocene warmth, Nature, 496, 43–49, 2013.

Griffin, D. L.: The late Neogene Sahabi rivers of the Sahara and their climatic and environmental implications for the Chad Basin, J. Geol. Soc. Lond., 163, 905–921, 2006.

Haywood, A. M., Dowsett, H. J., Otto-Bliesner, B., Chandler, M. A., Dolan, A. M., Hill, D. J., Lunt, D. J., Robinson, M. M., Rosenbloom, N., Salzmann, U., and Sohl, L. E.: Pliocene Model Intercomparison Project (PlioMIP): experimental design and boundary conditions (Experiment 1), Geosci. Model Dev., 3, 227–242, 2010.

Haywood, A. M., Dowsett, H. J., Robinson, M. M., Stoll, D. K., Dolan, A. M., Lunt, D. J., Otto-Bliesner, B., and Chandler, M. A.: Pliocene Model Intercomparison Project (PlioMIP): experimental design and boundary conditions (Experiment 2), Geosci. Model Dev., 4, 571–577, 2011.

Haywood, A. M., Hill, D. J., Dolan, A. M., Otto-Bliesner, B. L., Bragg, F., Chan, W.-L., Chandler, M. A., Contoux, C., Dowsett, H. J., Jost, A., Kamae, Y., Lohmann, G., Lunt, D. J., Abe-Ouchi, A., Pickering, S. J., Ramstein, G., Rosenbloom, N. A., Salzmann, U., Sohl, L., Stepanek, C., Ueda, H., Yan, Q., and Zhang, Z.: Large-scale features of Pliocene climate: results from the Pliocene Model Intercomparison Project, Clim. Past, 9, 191–209, 2013.

Haywood, A. M., Dowsett, H. J., and Dolan, A. M.: Integrating geological archives and climate models for the mid-Pliocene warm period, Nature Comm., 7, 10646, 2016a.

Haywood, A. M., Dowsett, H. J., Dolan, A. M., Rowley, D., Abe-Ouchi, A., Otto-Bliesner, B., Chandler, M. A., Hunter, S. J., Lunt, D. J., Pound, M., and Salzmann, U.: The Pliocene Model Intercomparison (PlioMIP) Phase 2: scientific objectives and experimental design, Clim. Past, 12, 663–675, 2016b.

Hill, D. J., Haywood, A. M., Lunt, D. J., Hunter, S. J., Bragg, F. J., Contoux, C., Stepanek, C., Sohl, L., Rosenbloom, N. A., Chan, W.-L., Kamae, Y., Zhang, Z., Abe-Ouchi, A., Chandler, M. A., Jost, A., Lohmann, G., Otto-Bliesner, B. L., Ramstein,

G., and Ueda, H.: Evaluating the dominant components of warming in Pliocene climate simulations, Clim. Past, 10, 79–90, 2014.

Howell, F. W., Haywood, A. M., Otto-Bliesner, B. L., Bragg, F., Chan, W.-L., Chandler, M. A., Contoux, C., Kamae, Y., A be-Ouchi, A., Rosenbloom, N. A., Stepanek, C., and Zhang Z.: Arctic sea ice simulation in the PlioMIP ensemble, Clim. Past, 12, 749–767, 2016.

Hu, A., Meehl, G. A., Han, W., Otto-Bliestner, B., Abe-Ouchi, A., and Rosenbloom, N.: Effects of the Bering Strait closure on AMOC and global climate under different background climates, Prog. Oceanogr., 132, 174–196, 2015.

Kageyama, M., Braconnot, P., Harrison, S. P., Haywood, A. M., Jungclaus, J., Otto-Bliesner, B. L., Peterschmitt, J.-Y., Abe-Ouchi, A., Albani, S., Bartlein, P. J., Brierley, C., Crusifix, M., Dolan, A., Fernandez-Donado, L., Fischer, H., Hopcroft, P. O., Ivanovic, R. F., Lambert, F., Lunt, D. J., Mahowald, N. M., Peltier, W. R., Phipps, S. J., Roche, D. M., Schmidt, G. A., Tarasov, L., Valdes, P. J., Zhang, Q., and Zhou, T.: PMIP4-CMIP6: the contribution of the Paleoclimate Modelling Intercomparison Project to CMIP6, Geosci., Model Dev. Discuss., doi:10.5194/gmd-2016-106, 2016.

Kamae, Y. and Ueda, H.: Evaluation of simulated climate in lower latitude regions during the mid-Pliocene warm period using paleovegetation data, SOLA, 7, 177–180, doi:10.2151/sola.2011-045, 2011.

Kamae, Y. and Ueda, H.: Mid-Pliocene global climate simulation with MRI-CGCM2.3: set-up and initial results of PlioMIP Experiments 1 and 2, Geosci. Model Dev., 5, 793–808, 2012.

Kamae, Y., Ueda, H., and Kitoh, A.: Hadley and Walker circulations in the mid-Pliocene warm period simulated by an atmospheric general circulation model, J. Meteorol. Soc. Japan, 89, 475–493, 2011.

Kamae, Y., Watanabe, M., Kimoto, M., and Shiogama, H.: Summertime land-sea thermal contrast and atmospheric circulation over East Asia in a warming climate–Part II: Importance of CO_2-induced continental warming, Clim. Dyn., 43, 2569–2583, 2014.

Kang, S. M., Frierson, D. M. W., and Held, I. M.: The tropical response to extratropical thermal forcing in an idealized GCM: the importance of radiative feedbacks and convective parameterization, J. Atmos. Sci., 66, 2812–2827, 2009.

Klein, S. A., Zhang, Y., Zelinka, M. D., Pincus, R., Boyle, J., and Gleckler, P. J.: Are climate model simulations of clouds improving? An evaluation using the ISCCP simulator, J. Geophys. Res. Atmos., 118, 1329–1342, 2013.

Koenig, S. J., Dolan, A. M., de Boer, B., Stone, E. J., Hill, D. J., DeConto, R. M., Abe-Ouchi, A., Lunt, D. J., Pollard, D., Quiquet, A., Saito, F., Savage, J., and van de Wal, R.: Ice sheet model dependency of the simulated Greenland Ice Sheet in the mid-Pliocene, Clim. Past, 11, 369–381, 2015.

Lisiecki, L. E. and Raymo, M. E.: A Pliocene-Pleistocene stack of 57 globally distributed benthic $\delta^{18}O$ records, Paleoceanography, 20, PA1003, 2005.

Li, X., Jiang, D., Zhang, Z., Zhang, R., Tian, Z., and Qing, Y.: Mid-Pliocene westerlies from PlioMIP simulations, Adv. Atmos. Sci., 32, 909–923, 2015.

Manabe, S., Stouffer, R. J., Spelman, M. J., and Bryan, K.: Transient responses of a coupled ocean-atmosphere model to gradual changes of atmospheric CO_2. Part I: annual mean response, J. Clim., 4, 785–818, 1991.

Masson-Delmotte, V., Schulz, M., Abe-Ouchi, A., Beer, J., Ganopolski, A., González Rouco, J. F., Jansen, E., Lambeck, K., Luterbacher, J., Naish, T., Osborn, T., Otto-Bliesner, B., Quinn, T., Ramesh, R., Rojas, M., Shao, X., and Timmermann, A.: Information from Paleoclimate Archives. In: Climate Change 2013: The Physical Science Basis. Contribution of Working Group I to the Fifth Assessment Report of the Intergovernmental Panel on Climate Change [Stocker, T.F., et al. (eds.)]. Cambridge University Press, Cambridge, United Kingdom and New York, NY, USA, pp. 383–464, 2014.

Mizuta, R.: Intensification of extratropical cyclones associated with the polar jet change in the CMIP5 global warming projections, Geophys. Res. Lett., 39, L19707, doi:10.1029/2012GL053032, 2012.

Motoi, T., Chan, W.-L., Minobe, S., and Sumata, H.: North Pacific halocline and cold climate induced by Panamanian Gateway closure in a coupled ocean-atmosphere GCM, Geophys. Res. Lett., 32, L10618, doi:10.1029/2005GL022844, 2005.

Naish, T., Powell, R., Levy, R.,Wilson, G., Scherer, R., Talarico, F., Krissek, L., Niessen, F., Pompilio, M., andWilson, T.: Obliquity-paced Pliocene West Antarctic ice sheet oscillations, Nature, 458, 322–328, 2009.

Pithan, F. and Mauritsen, T.: Arctic amplification dominated by temperature feedbacks in contemporary climate models, Nature Geosci., 7, 181–184, 2014.

Pollard, D. and DeConto, R. M.: Modelling West Antarctic ice sheet growth and collapse through the past five million years, Nature, 458, 329–332, 2009.

Pound, M. J., Tindall, J., Pickering, S. J., Haywood, A. M., Dowsett, H. J., and Salzmann, U.: Late Pliocene lakes and soils: a global data set for the analysis of climate feedbacks in a warmer world, Clim. Past, 10, 167–180, 2014.

Raymo, M. E., Grant, B., Horowitz, M., and Rau, G. H.: Mid-Pliocene warmth: Stronger greenhouse and stronger conveyor, Mar. Micropaleontol., 27, 313–326, 1996.

Raymo, M. E., Mitrovica, J. X., O'Leary, M. J., DeConto, R. M., and Hearty, P. J.: Departures from eustasy in Pliocene sea level records, Nature Geosci., 4, 328–332, 2011.

Reichler, T. and Kim, J.: How well do coupled models simulate today's climate? Bull. Amer. Meteor. Soc., 89, 303–311, 2008.

Robinson, M. M.: New quantitative evidence of extreme warmth in the Pliocene Arctic, Stratigraphy, 6, 265–275, 2009.

Robinson, M. M., Valdes, P. J., Haywood, A. M., Dowsett, H. J., Hill, D. J., and Jones, S. M.: Bathymetric controls on Pliocene North Atlantic and Arctic sea surface temperature and deepwater production, Palaeogeogr. Palaeocl., 309, 92–97, 2011.

Rowley, D. B., Forte, A. M., Moucha, R., Mitrovica, J. X., Simmons, N. A., and Grand, S. P.: Dynamic topography change of the eastern United States since 3 million years ago, Science, 340, 1560–1563, 2013.

Salzmann, U., Haywood, A. M., Lunt, D., Valdes, P., and Hill, D.: A new global biome reconstruction and data-model comparison for the middle Pliocene, Global Ecol. Biogeogr., 17, 432–447, 2008.

Salzmann, U., Dolan, A. M., Haywood, A. M., Chan, W.-L., Voss, J., Hill, D. J., Abe-Ouchi, A., Otto-Bliesner, B., Bragg, F. J., Chandler, M. A., Contoux, C., Dowsett, H. J., Jost, A., Kamae, Y., Lohmann, G., Lunt, D. J., Pickering, S. J., Pound, M.

J., Ramstein, G., Rosenbloom, N. A., Sohl, L., Stepanek, C., Ueda, H., and Zhang, Z.: Challenges in quantifying Pliocene terrestrial warming revealed by data-model discord, Nature Clim. Change, 3, 969–974, 2013.

Sato, N., Sellers, P. J., Randall, D. A., Schneider, E. K., Shukla, J., Kinter, J. L., Hou, Y.-Y., and Albertazzi, E.: Effects of implementing the simple biosphere model in a general circulation model, J. Atmos. Sci., 46, 2757–2782, 1989.

Schuster, M., Duringer, P., Ghienne, J.-F., Bernard, A., Brunet, M., Vignaud, P., and Mackaye, H. T.: The Holocene Lake MegaChad: extension, dynamic and palaeoenvironmental implications since upper Miocene, 11th European Union of Geoscience Meeting, Strasbourg, 2001.

Schuster, M., Duringer, P., Ghienne, J.-F., Vignaud, P., Mackaye, H. T., Likius, A., and Brunet, M.: The age of the Sahara desert, Science, 311, 821–822, 2006.

Seki, O., Foster, G. L., Schmidt, D. N., Mackensen, A., Kawamura, K., and Pancost, R. D.: Alkenone and boron-based Pliocene pCO_2 records, Earth Planet. Sci. Lett., 292, 201–211, 2010.

Sellers, P. J., Mintz, Y., Sud, Y. C., and Dalcher, A.: A simple biosphere model (SiB) for use within general circulation models, J. Atmos. Sci., 43, 505–531, 1986.

Serreze, M. C. and Barry, R. G.: Processes and impacts of Arctic amplification: A research synthesis, Global Planet. Change, 77, 85–96, 2011.

Shiogama, H., Stone, D. A., Nagashima, T., Nozawa, T., and Emori, S.: On the linear additivity of climate forcing-response relationships at global and continental scales, Int. J. Climatol., 33, 2542–2550, 2013.

Sohl, L. E., Chandler, M. A., Schmunk, R. B., Mankoff, K., Jonas, J. A., Foley, K. M., and Dowsett, H. J.: PRISM3/GISS topographic reconstruction: U. S. Geological Survey Data, Series 419, 6 pp., 2009.

Speer, K., and Tziperman, E.: Rates of water mass formation in the North Atlantic Ocean, J. Phys. Oceanogr., 22, 93–104, 1992.

Sun, Y., Ramstein, G., Contoux, C., and Zhou, T.: A comparative study of large-scale atmospheric circulation in the context of a future scenario (RCP4.5) and past warmth (mid-Pliocene), Clim. Past, 9, 1613–1627, 2013.

Ulbrich, U., Leckebusch, G. C., and Pinto, J. G.: Extra-tropical cyclones in the present and future climate: A review, Theor. Appl. Climatol., 96, 117–131, 2009.

Wang,W.-C., Ling, X.-Z., Dudek, M. P., Pollard D., and Thompson, S. L.: Atmospheric ozone as a climate gas, Atmos. Res., 37, 247–256, 1995.

Wara, M., Ravelo, A. C., and Delaney, M. L.: Permanent El Niño conditions during the Pliocene warm period, Science, 309, 758–761, 2005.

Willeit, M., Ganopolski, A., and Feulner, G.: On the effect of orbital forcing on mid-Pliocene climate, vegetation and ice sheets, Clim. Past, 9, 1749–1759, 2013.

Xie, S.-P., Xu, H., Saji, N. H., Wang, Y., and Liu, W. T.: Role of narrow mountains in large-scale organization of Asian monsoon convection, J. Clim., 19, 3420–3429, 2006.

Xie, S.-P., Deser, C., Vecchi, G. A., Collins, M., Delworth, T. L., Hall, A., Hawkins, E., Johnson, N. C., Cassou, C., Giannini, A., and Watanabe, M.: Towards predictive understanding of regional climate change, Nature Clim. Change, 5, 921–930, 2015.

Yoshimori, M., Watanabe, M., Abe-Ouchi, A., Shiogama, H., and Ogura, T.: Relative contribution of feedback processes to Arctic amplification of temperature change in MIROC GCM. Clim. Dyn., 42, 1613–1630, 2014.

Yukimoto, S., Noda, A., Kitoh, A., Hosaka, M., Yoshimura, H., Uchiyama, T., Shibata, K., Arakawa, O., and Kusunoki, S.: Present-day and climate sensitivity in the meteorological research institute coupled GCM version 2.3 (MRI-CGCM2.3), J. Meteorol. Soc. Japan, 84, 333–363, 2006.

Zhang, R. and Delworth, T. L.: Impact of Atlantic multidecadal oscillations on India/Sahel rainfall and Atlantic hurricanes, Geophys. Res. Lett., 33, L17712, doi:10.1029/2006GL026267, 2006.

Zhang, R., and Jiang, D.: Impact of vegetation feedback on the mid-Pliocene warm climate, Adv. Atmos. Sci., 31, 1407–1416, 2014.

Zhang, R., Yan, Q., Zhang, Z. S., Jiang, D., Otto-Bliesner, B. L., Haywood, A. M., Hill, D. J., Dolan, A. M., Stepanek, C., Lohmann, G., Contoux, C., Bragg, F., Chan,W.-L., Chandler, M. A., Jost, A., Kamae, Y., Abe-Ouchi, A., Ramstein, G., Rosenbloom, N. A., Sohl, L., and Ueda, H.: Mid-Pliocene East Asian monsoon climate simulated in the PlioMIP, Clim. Past, 9, 2085–2099, 2013.

Zhang, Z.-S., Nisancioglu, K. H., Chandler, M. A., Haywood, A. M., Otto-Bliesner, B. L., Ramstein, G., Stepanek, C., Abe-Ouchi, A., Chan,W.-L., Bragg, F. J., Contoux, C., Dolan, A. M., Hill, D. J., Jost, A., Kamae, Y., Lohmann, G., Lunt, D. J., Rosenbloom, N. A., Sohl, L. E., and Ueda, H.: Mid-pliocene Atlantic Meridional Overturning Circulation not unlike modern, Clim. Past, 9, 1495–1504, 2013.

Table 1: Summary of model and experimental setting.

Model	MRI-CGCM2.3
Paleogeography	Standard
Dynamic vegetation	No
Carbon cycle	No
Dynamical lake	No
CH_4	760 ppbv
N_2O	270 ppbv
Ozone	Wang et al. (1995)
Solar constant	1365 W m^{-2}
Eccentricity	0.016724
Obliquity	23.446°
Perihelion	102.04°
Integration length	500 years

Table 2: Details of six PlioMIP2 experiments examined in this study. PlioMIP1 Pliocene run represents AOGCM_NFA run in Kamae and Ueda (2012). Soil and land–sea mask are identical among all the experiments.

Experiments	Orography, lakes	Vegetation	Ice sheet	CO_2 (ppmv)
E280 (Pre-industrial)	Modern	Modern	Modern	280
E400	Modern	Modern	Modern	400
E560	Modern	Modern	Modern	560
Ei280	Modern	Modern	Pliocene	280
Eo280	Pliocene	Pliocene	Modern	280
Eoi400 (Pliocene)	Pliocene	Pliocene	Pliocene	400
PlioMIP1 Pliocene	PlioMIP1 orography, modern lake	Pliocene	PlioMIP1	405

Table 3: Anomalies in global-mean surface air temperature (Δ*SAT*; °C) in the PlioMIP2 runs relative to E280. The anomalies are calculated by averages for the last 50-yr of the individual runs.

Experiments	Global-mean Δ*SAT* (°C)
E400	1.7
E560	2.8
Ei280	0.3
Eo280	0.5
Eoi400	2.4
PlioMIP1	1.8

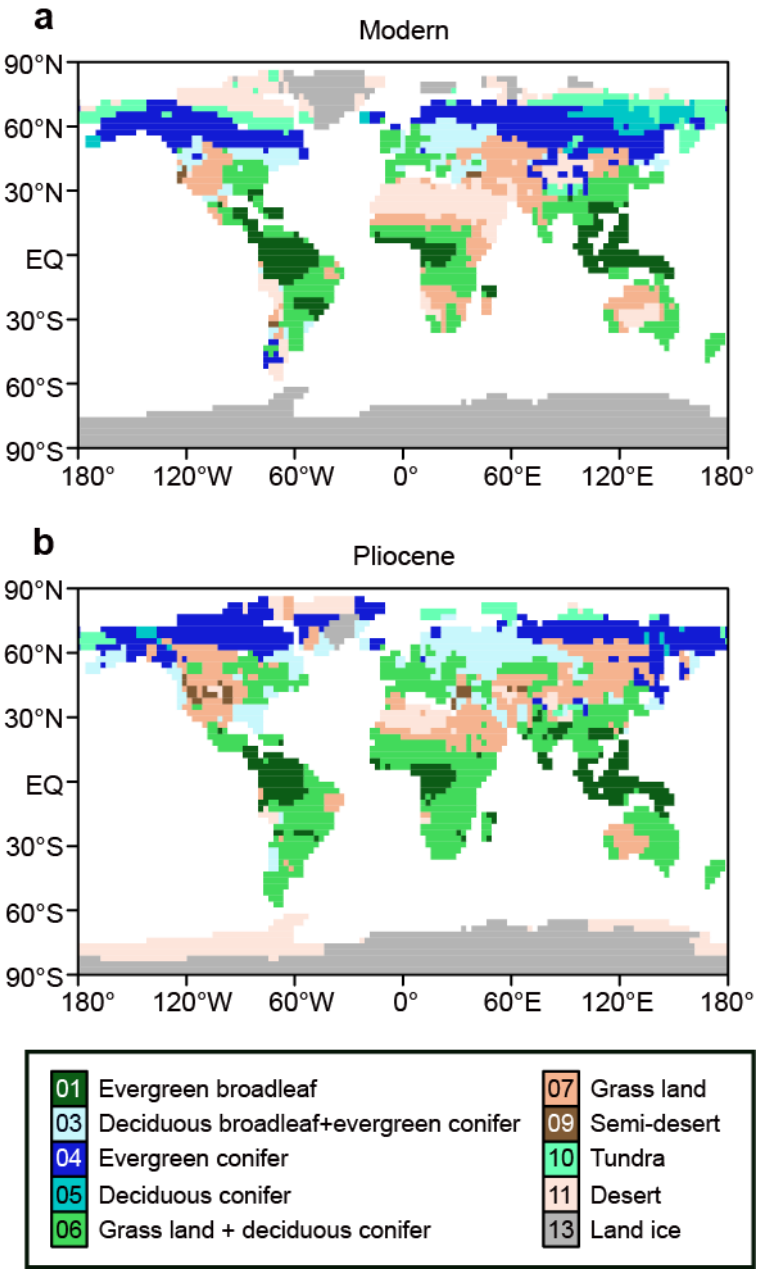

Figure 1: Prescribed land cover (SiB2 classification) for (a) modern and (b) Pliocene conditions.

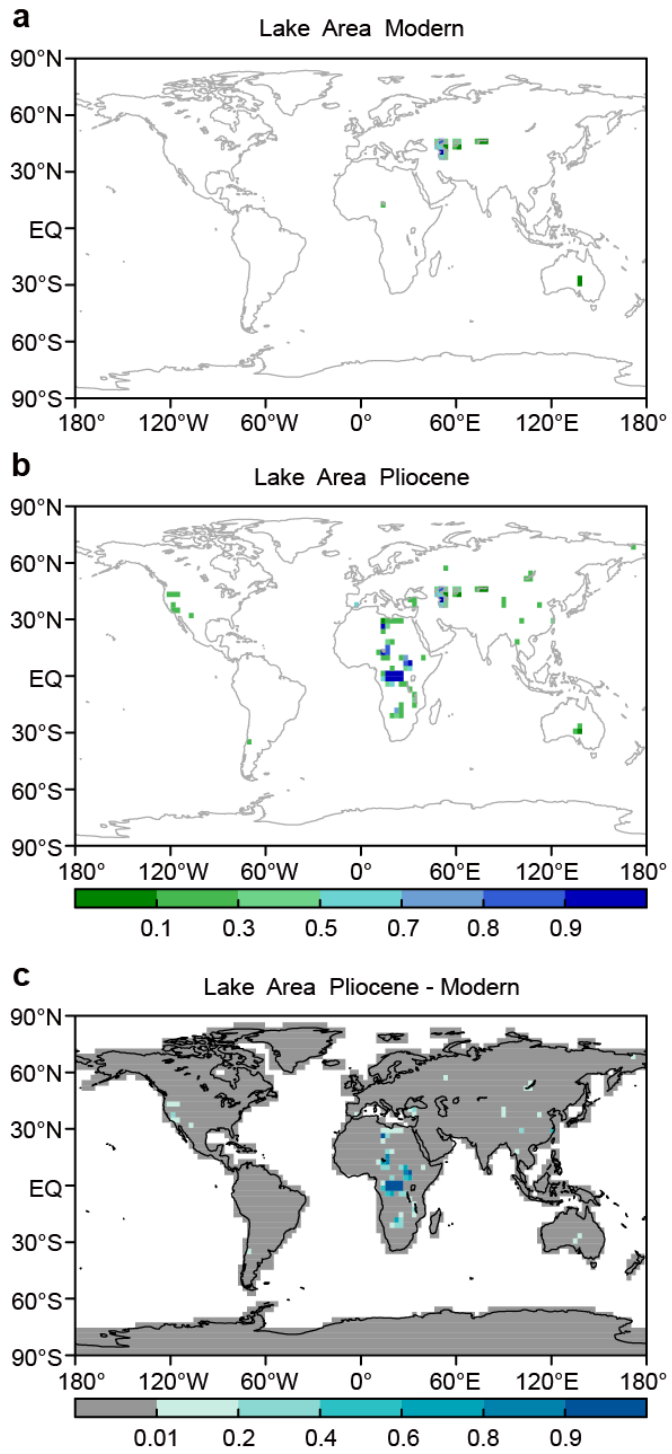

Figure 2: Prescribed lake area fraction over land. (a) Modern, (b) Pliocene, and (c) Pliocene minus modern.

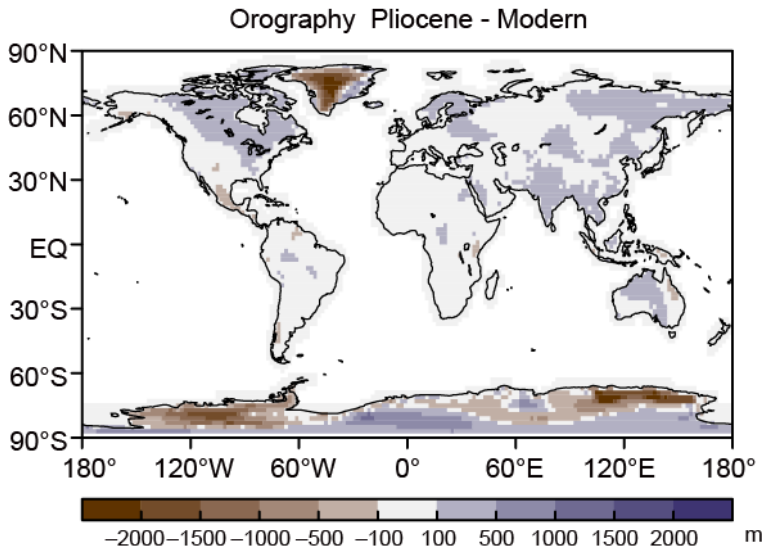

Figure 3: Prescribed anomaly in land orography (m) for Pliocene relative to modern.

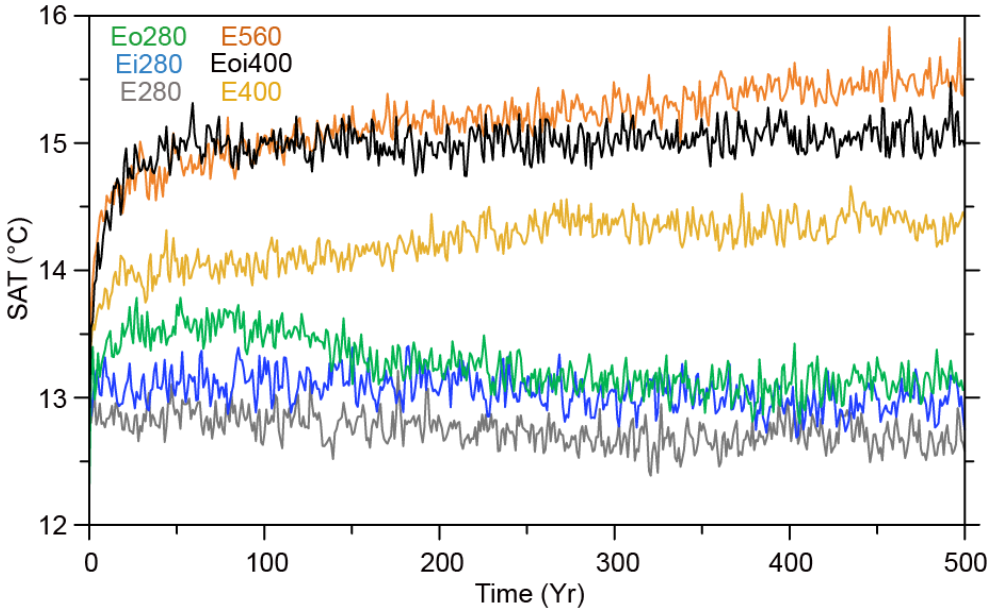

Figure 4: Time evolution of annual-mean global-mean surface air temperature (SAT; °C) in each run.

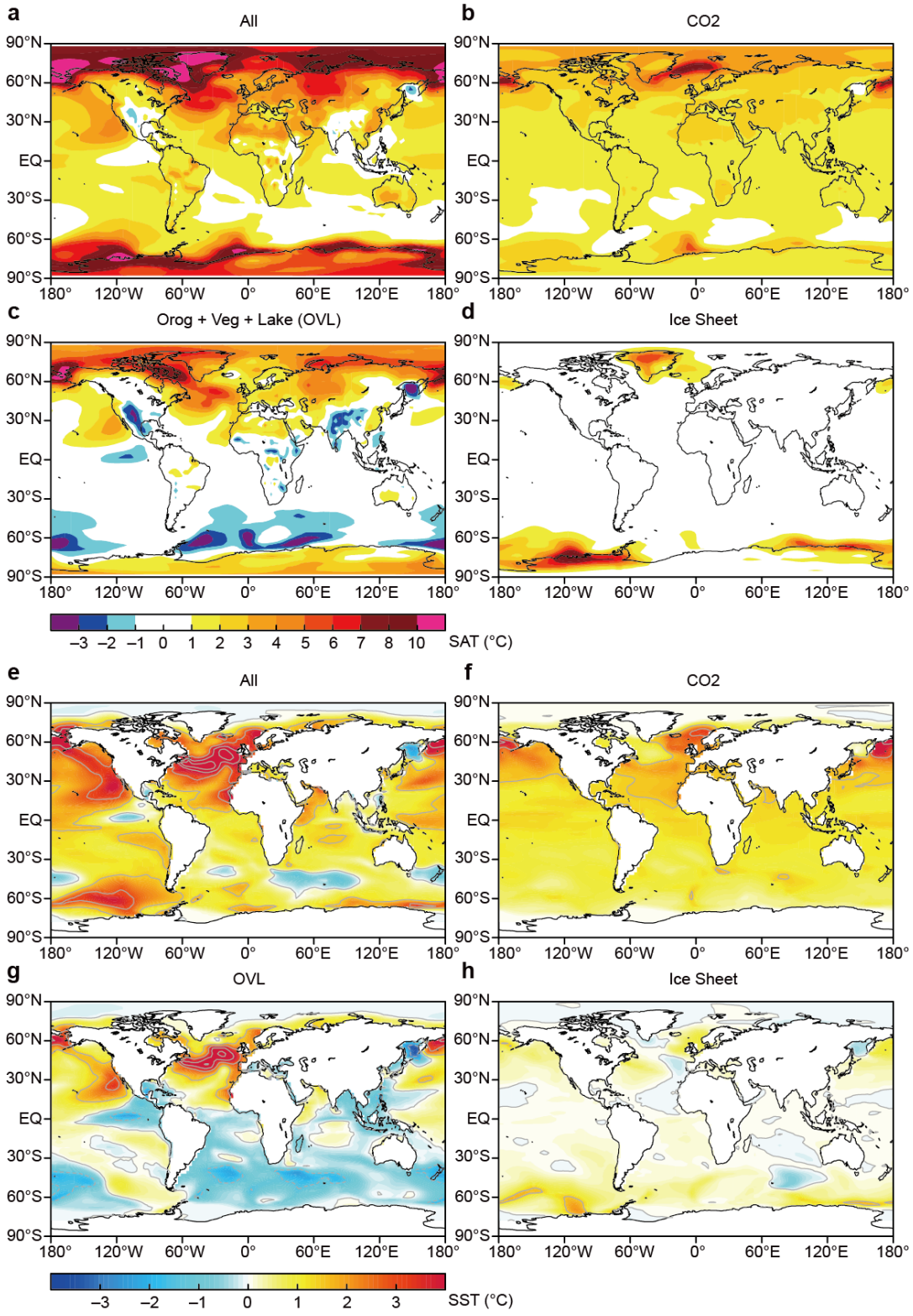
a
All
b
CO2
c
Orog + Veg + Lake (OVL)
d
Ice Sheet
90°N
60°N
30°N
EQ
30°S
60°S
90°S
180°
120°W
60°W
0°
60°E
120°E
180°
−3 −2 −1 0 1 2 3 4 5 6 7 8 10
SAT (°C)
e
All
f
CO2
g
OVL
h
Ice Sheet
−3 −2 −1 0 1 2 3
SST (°C)

Figure 5: (a) Anomaly in SAT (°C) in Pliocene run relative to pre-industrial run (hereafter *All*). (b) E400 run minus pre-industrial run (*CO2*), (c) Eo280 run minus pre-industrial run (*OVL*), and (d) Ei280 run minus pre-industrial run (*Ice Sheet*), respectively. The anomalies are calculated by averages for the last 50-yr of the individual runs. (e–h) Similar to (a–d), but for sea surface temperature (SST; °C). Intervals of grey contours are 1.5 °C.

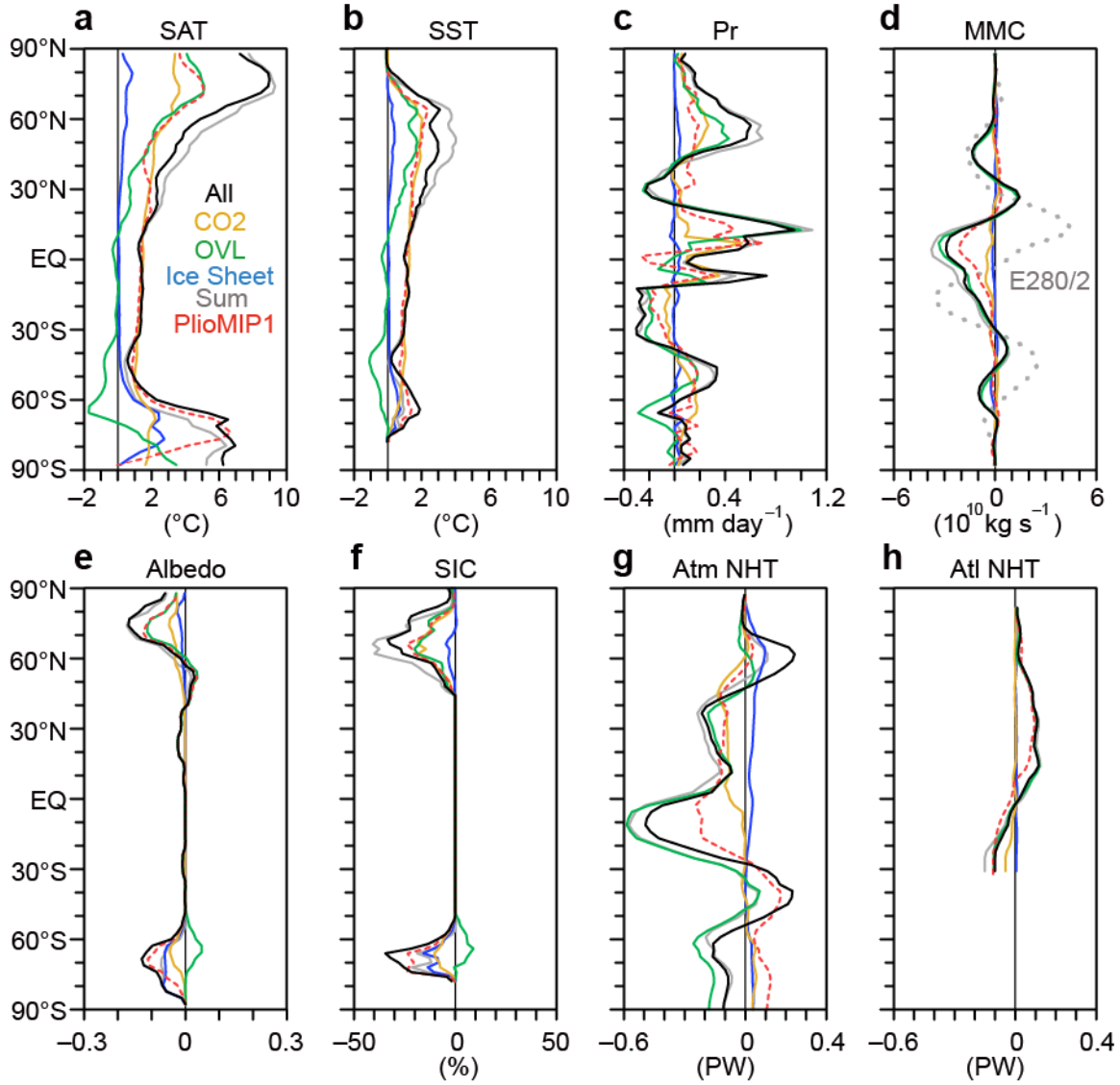

Figure 6: Zonal-mean anomalies in (a) SAT (°C), (b) SST (°C), (c) precipitation (mm day^{-1}), (d) mass stream function of mean meridional circulation at 500 hPa level (10^{10} kg s^{-1}), (e) surface albedo, (f) sea ice concentration (%), (g) northward heat transport due to atmosphere (PW) and (h) the Atlantic (PW). Black, yellow, green, and blue lines represent *All*, *CO2*, *OVL*, and *Ice Sheet*, respectively. Grey line represents *Sum*. Dashed red lines represent results of AOGCM_NFA run conducted in the identical model in PlioMIP1 (Kamae and Ueda, 2012). Dotted grey line in (g) represents climatology in pre-industrial run multiplied by 0.5.

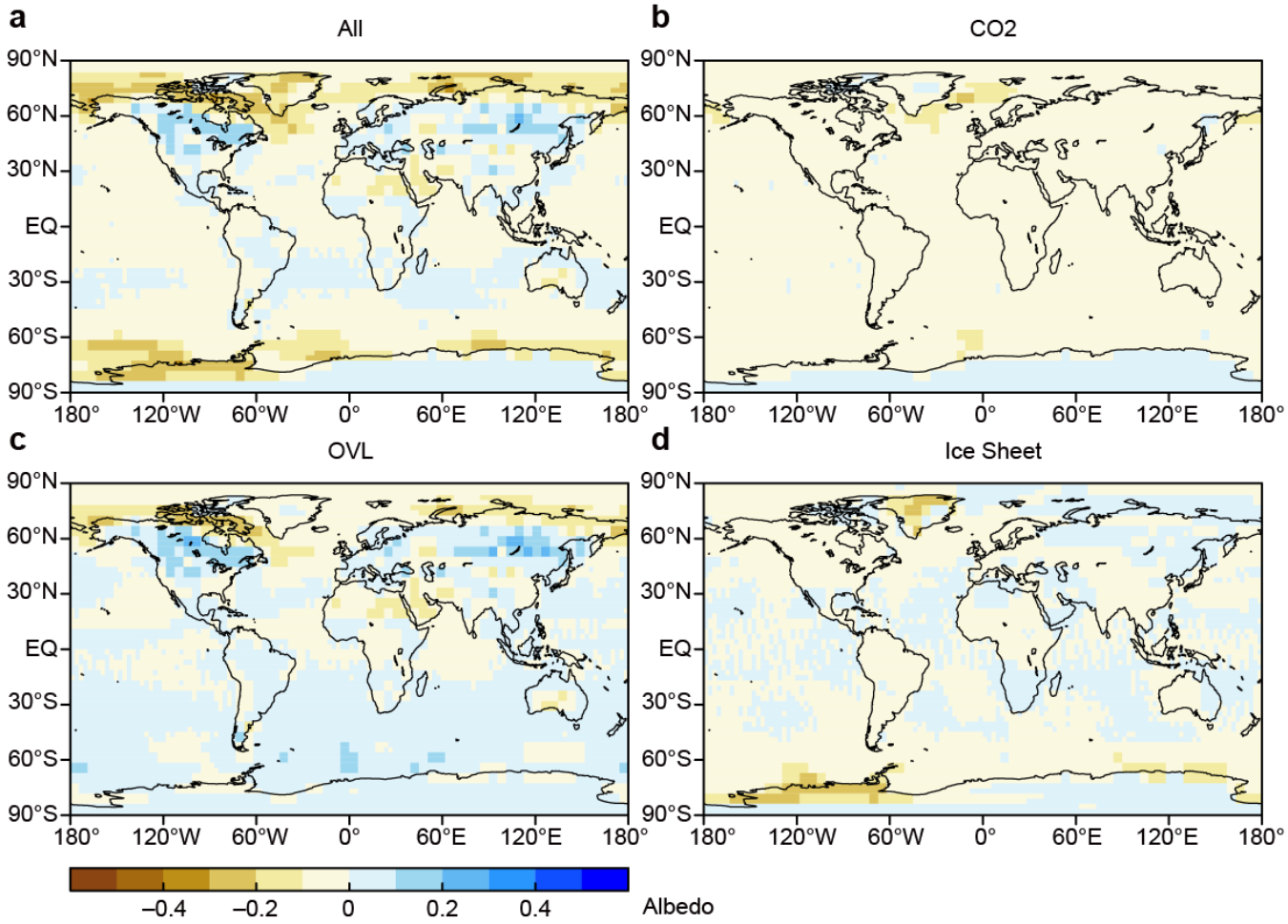

Figure 7: Similar to Fig. 5, but for surface albedo.

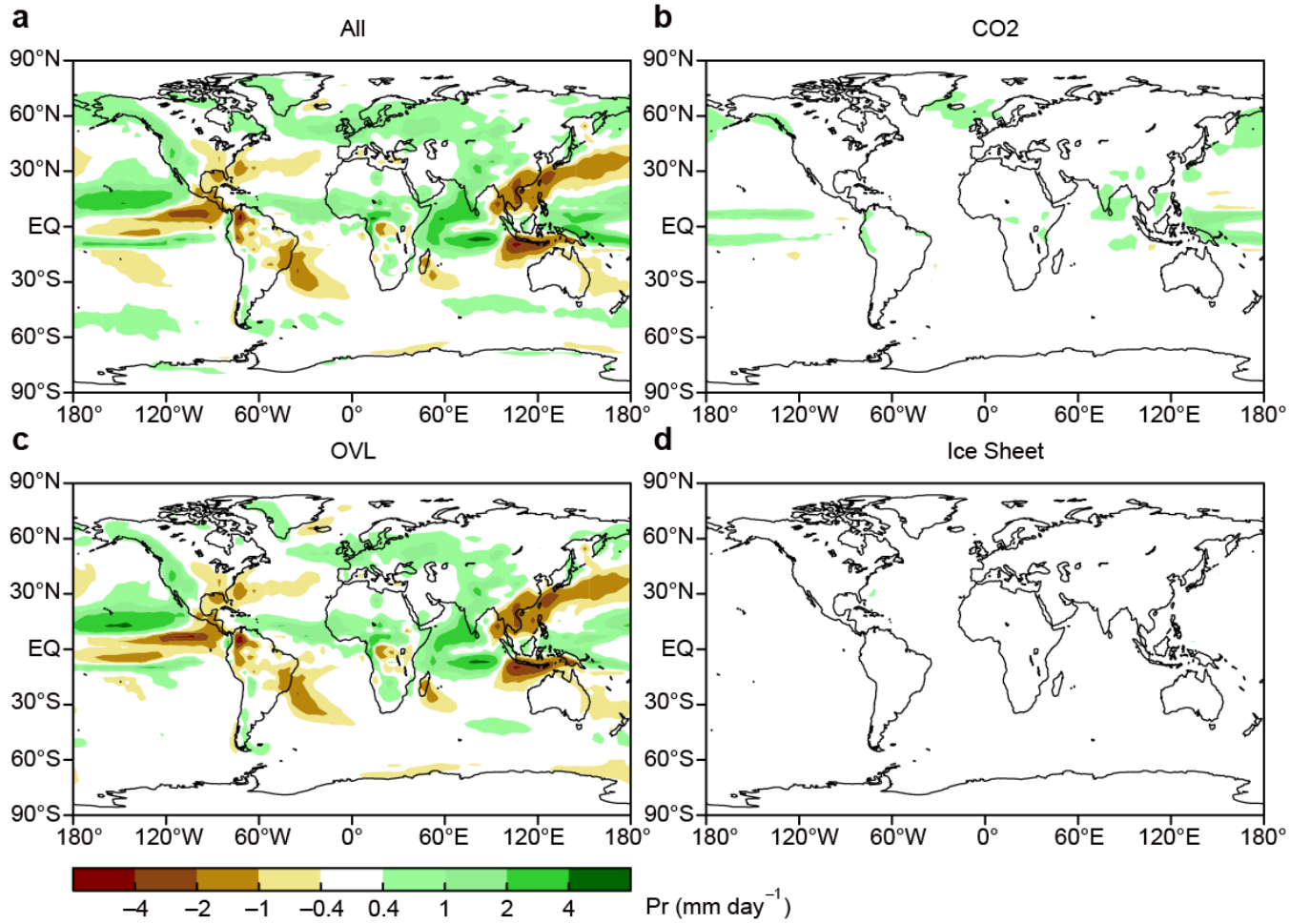

Figure 8: Similar to Fig. 5, but for precipitation (mm day^{-1}).

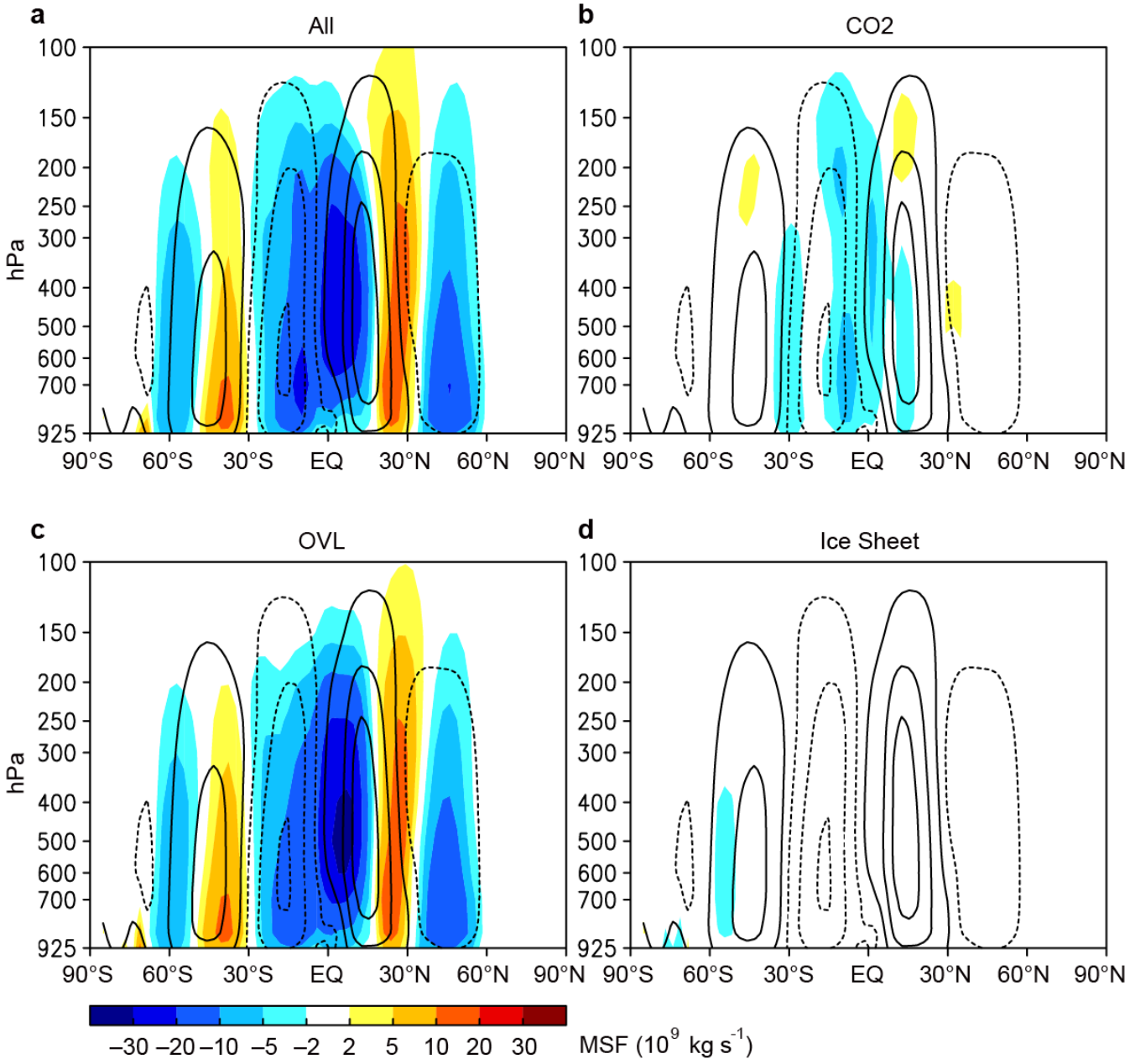

Figure 9: Anomalies in mass stream function of mean meridional circulation (10^9 kg s^{-1}). (a) *All* (shading). Contours represent climatological mass stream function in pre-industrial run (±10, 40, 70 10^9 kg s^{-1}). Solid and dashed contours represent positive and negative anomalies, respectively. (b) *CO2*, (c) *OVL*, and (d) *Ice Sheet*, respectively.

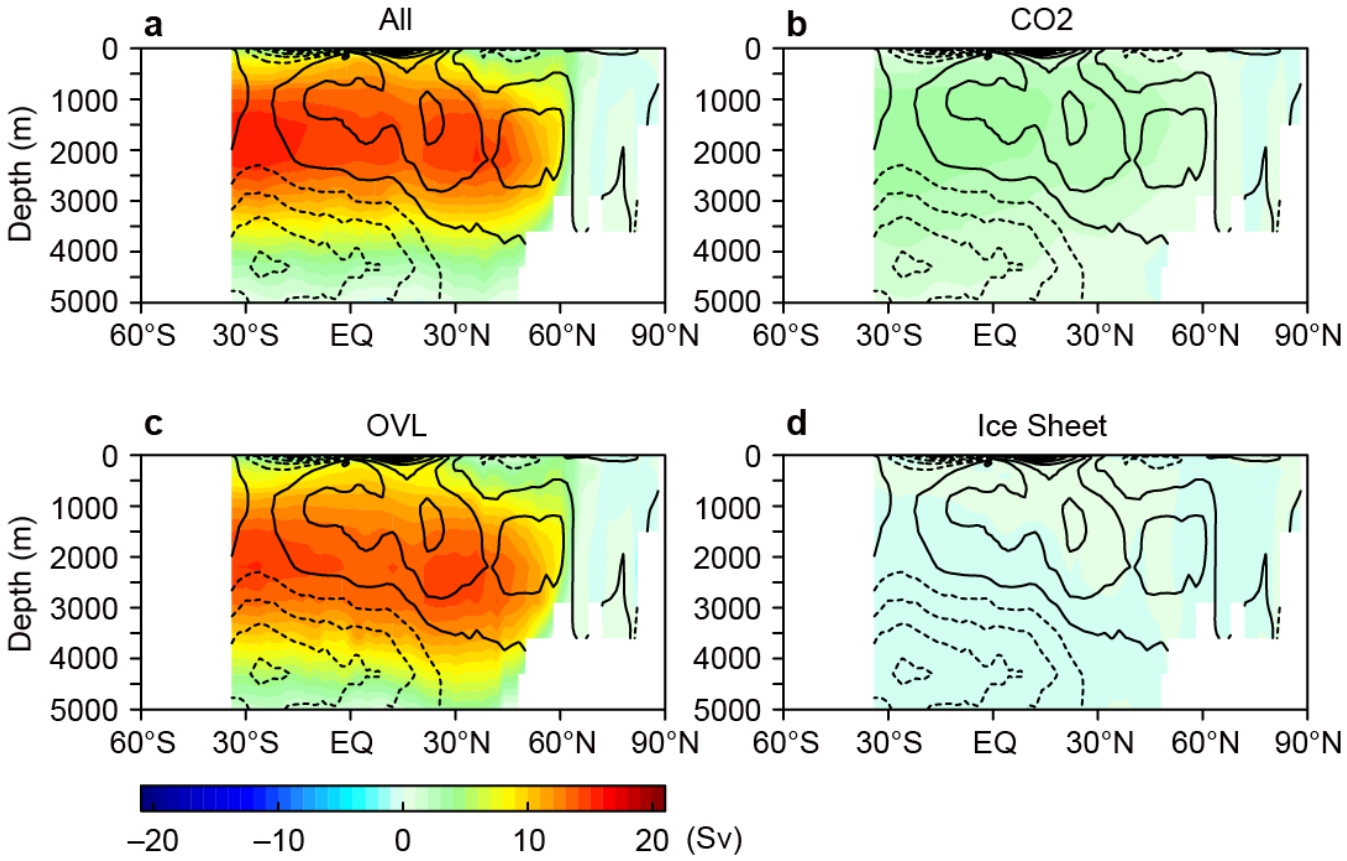

Figure 10: Anomalies in Atlantic meridional overturning circulation (AMOC; shading; Sv). Contours represent climatological overturning circulation in pre-industrial run (±0, 2, 4, 6, 8 Sv). (a) *All*, (b) *CO2*, (c) *OVL*, and (d) *Ice Sheet*, respectively.

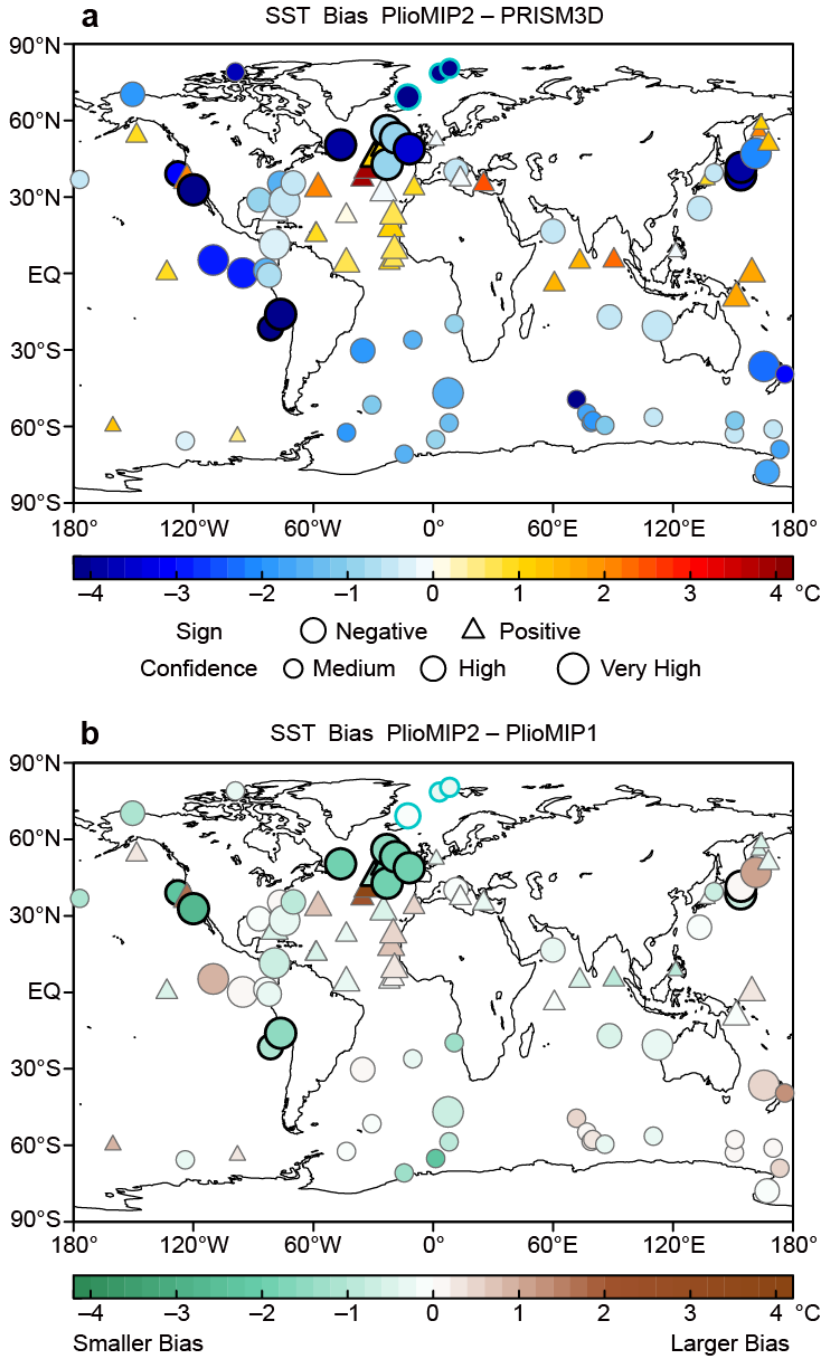

Figure 11: (a) SST bias (°C) in PlioMIP2 Pliocene run compared with PRISM3D proxy-based SST reconstruction (Dowsett et al., 2009). Coloured circles and triangles represent cool and warm biases, respectively. Sizes of plots indicate confidence levels of SST estimate based on chronology, sampling density, sampling quality and performance of quantitative method (Dowsett et al., 2013). Thick black and blue open circles indicate proxy sites in which estimated SST anomalies are large (between 4.0 and 8.9 °C) and extremely large (> 8.9 °C), respectively. (b) Comparison of SST biases in Pliocene runs between PlioMIP2 and 1. Coloured plots indicate differences in absolute biases between the two.

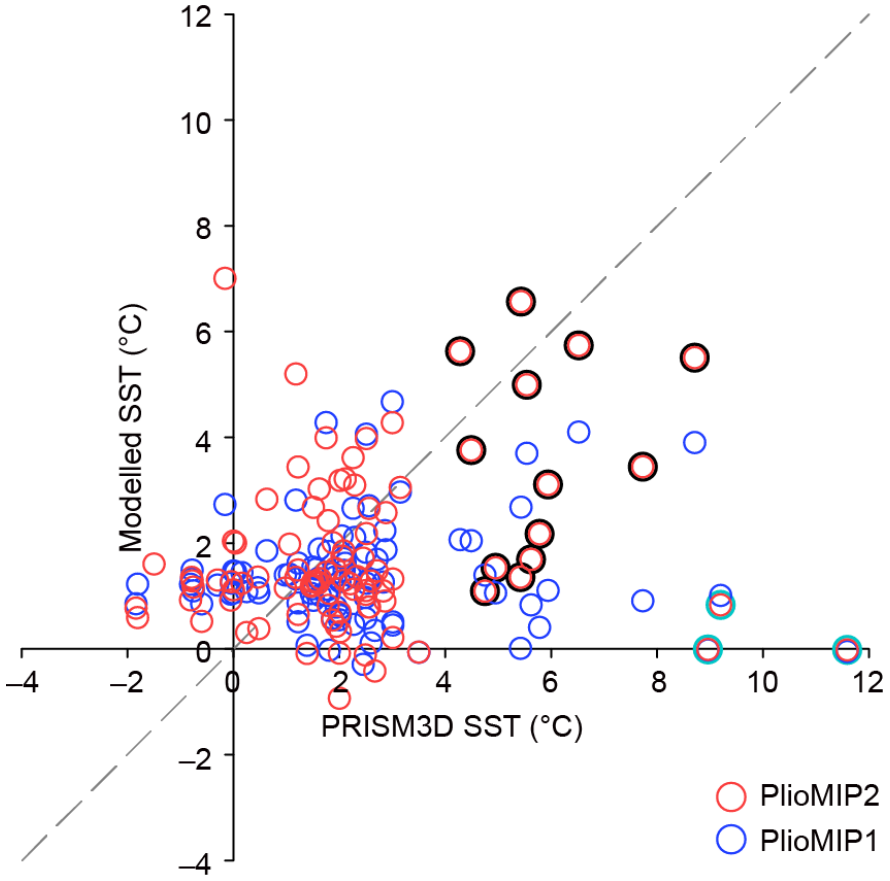

Figure 12: Scatter diagram of proxy-based SST reconstruction (°C) and simulated SST (°C). Red and blue circles represent Pliocene runs in PlioMIP2 and 1, respectively. Thick black and blue open circles are identical to Fig. 11. Dashed grey line represents one-by-one line.

5